

omers, representing a significant improvement over the original ASP-W results (which were already fairly good).

From Table 1 we find very good agreement between the two lowest tunneling barriers on VRT (ASP-W) and ab initio calculations (5, 23), indicating that the topological features of the 6D IPS are adequately represented. The highest barrier (for bifurcation), which is not explicitly constrained in the fit, may be too small on VRT (ASP-W), but it is difficult to ascertain this given the large variations in ab initio values. In general, we clearly see significant improvements in the barrier heights relative to those on the ASP-W surface, indicating that the hydrogen bond rearrangement dynamics in the dimer will be properly represented.

To further characterize VRT (ASP-W), we have computed both equilibrium and vibrationally averaged ground state structures, D_e , and D_0 for cyclic D_2O trimers and tetramers, which have been characterized by terahertz laser spectroscopy (3). This was done using DQMC on a trimer (tetramer) IPS constructed by pairwise addition of the pair potentials, followed by computing first-order, iterated, n -body induction. As shown in Table 2, good agreement is found with both ab initio and experimental results, and again a significant improvement relative to ASP-W is found, which generally produced O–O distances that were too long. Effective pair potentials, such as TIP4P, are not able to reproduce the cluster features, yielding rather short O–O distances and binding energies that are too large. That a pair potential such as VRT (ASP-W) does so well in calculating properties of larger clusters is not entirely unexpected, as the dominant n -body force is induction (polarization), which is explicitly treated by the polarizable VRT (ASP-W) potential. In contrast, effective pair potentials parameterize the many-body forces in an average way according to bulk properties and so are unable to simultaneously describe both small clusters and the bulk.

The principal weakness in the VRT (ASP-W) potential is the constraint of frozen water monomers to equilibrium properties. It is known that the donor O–H bond actually elongates slightly (<1%) upon hydrogen bond formation, accompanied by smaller changes in the bond angle (24, 25). Although these subtle effects must eventually be included to obtain a “perfect” water pair potential, to do so requires a complete 12D treatment of the VRT dynamics and potential surface, which currently transcends the state of the art. Preliminary explorations indicate that the main effects of including monomer nonrigidity involve some reduction in the acceptor switching splitting and a small (~0.1 kcal/mol) increase in D_e . In any case, we expect the effects of monomer nonrigidity on the fitted potential to be relatively minor

(25); VRT (ASP-W) is clearly quite close to the “exact” water pair potential. Moreover, as computational power continues to increase, it will ultimately become possible to determine the small exchange-repulsion and dispersion contributions to the many-body interactions (26) that are operative within aggregates of water molecules, as well as to further refine subtle features of the pair potential by comparing results computed rigorously from this pair potential with the precise VRT data measured for the water trimer, tetramer, pentamer, and hexamer. Hence, a truly rigorous molecular description of the force fields of solid and liquid water seems close at hand.

References and Notes

- S. Solomon, R. W. Portman, R. W. Sanders, J. S. Daniel, *J. Geophys. Res.* **103**, 3847 (1998).
- G. T. Fraser, *Int. Rev. Phys. Chem.* **10**, 189 (1991).
- K. Liu, J. D. Cruzan, R. J. Saykally, *Science* **271**, 929 (1996) and references therein.
- R. J. Saykally and G. A. Blake, *ibid.* **259**, 1570 (1993).
- B. J. Smith, D. J. Swanton, J. A. Pople, H. F. Schaefer, L. Radom, *J. Chem. Phys.* **92**, 1240 (1990).
- C. Millot and A. J. Stone, *Mol. Phys.* **77**, 439 (1992).
- The potential form and parameter sets are available at www.cchem.berkeley.edu/~rjsgrp/.
- N. Pugliano and R. J. Saykally, *J. Chem. Phys.* **96**, 1832 (1992).
- J. B. Paul, R. A. Provencal, R. J. Saykally, *J. Phys. Chem. A* **102**, 3279 (1998).
- C. Leforestier, L. B. Braly, K. Liu, M. J. Elrod, R. J. Saykally, *J. Chem. Phys.* **106**, 8527 (1997).
- R. S. Fellers, L. B. Braly, R. J. Saykally, C. Leforestier, *ibid.* **110**, 6306 (1999).
- M. J. Elrod and R. J. Saykally, *ibid.* **103**, 933 (1995).
- L. A. Curtiss, D. J. Frurip, M. Blander, *ibid.* **71**, 2703 (1979).
- J. R. Reimers, R. O. Watts, M. L. Klein, *Chem. Phys.* **64**, 95 (1982).
- M. W. Feyereisen, D. Feller, D. A. Dixon, *J. Phys. Chem.* **100**, 2993 (1996).
- E. M. Mas and K. Szalewicz, *J. Chem. Phys.* **104**, 7606 (1996).
- A. Halkier et al., *Theor. Chem. Acc.* **97**, 150 (1997).
- S. S. Xantheas, *J. Chem. Phys.* **110**, 4566 (1999) and references therein.
- J. K. Gregory and D. C. Clary, *ibid.* **102**, 7817 (1995).
- D. A. McQuarrie, in *Statistical Mechanics*, S. A. Rice, Ed. (Harper and Row, New York, 1976).
- G. S. Kell, G. E. McLaurin, E. Whalley, *Proc. R. Soc. London Ser. A* **425**, 49 (1989).
- C. Millot, J. C. Soetens, M. T. C. Martins-Costa, M. P. Hodges, A. J. Stone, *J. Phys. Chem. A* **102**, 754 (1998).
- D. J. Wales, in *Theory of Atomic and Molecular Clusters 2*, J. Jellick, Ed. (Springer-Verlag, Heidelberg, Germany, in press) (see <http://brian.ch.cam.ac.uk/publications.html>).
- S. Xantheas and T. H. Dunning, *J. Chem. Phys.* **99**, 8774 (1993).
- J. K. Gregory and D. C. Clary, *J. Phys. Chem.* **100**, 18014 (1998).
- M. J. Elrod and R. J. Saykally, *Chem. Rev.* **94**, 1975 (1994).
- J. A. Odutola and T. R. Dyke, *J. Chem. Phys.* **72**, 5062 (1980).
- E. N. Karyakin, G. T. Fraser, R. D. Suenram, *Mol. Phys.* **78**, 1179 (1993).
- A. J. Stone, A. Dullweber, P. L. A. Popelier, D. J. Wales, *Orient: A Program for Studying Interactions Between Molecules, Version 3.2* (University of Cambridge, Cambridge, 1995), available at <http://fandango.ch.cam.ac.uk/>.
- K. Liu, M. G. Brown, R. J. Saykally, *J. Phys. Chem. A* **101**, 8995 (1997).
- W. L. Jorgensen, J. Chandrasekhar, J. D. Madura, R. W. Impey, M. L. Klein, *J. Chem. Phys.* **79**, 926 (1983).
- We thank C. Millot and A. Stone for providing the source code of the ASP-W potential. Supported by the Experimental Physical Chemistry Program of NSF and the France-Berkeley Cooperative Grant Program.

22 December 1998; accepted 22 March 1999

Design and Self-Assembly of Open, Regular, 3D Mesostructures

Tricia L. Breen, Joe Tien,
Scott R. J. Oliver, Tanja Hadzic, George M. Whitesides*

Self-assembly provides the basis for a procedure used to organize millimeter-scale objects into regular, three-dimensional arrays (“crystals”) with open structures. The individual components are designed and fabricated of polyurethane by molding; selected faces are coated with a thin film of liquid, metallic alloy. Under mild agitation in warm, aqueous potassium bromide solution, capillary forces between the films of alloy cause self-assembly. The structures of the resulting, self-assembled arrays are determined by structural features of the component parts: the three-dimensional shape of the components, the pattern of alloy on their surfaces, and the shape of the alloy-coated surfaces. Self-assembly of appropriately designed chiral pieces generates helices.

We describe a procedure that uses self-assembly of patterned, three-dimensional (3D), mesoscale (millimeter- to centimeter-scale) objects

Department of Chemistry and Chemical Biology, Harvard University, 12 Oxford Street, Cambridge, MA 02138, USA.

*To whom correspondence should be addressed.

to generate open, regular, 3D structures. These types of structures may eventually find use as the cores of densely interconnected, 3D electronic and optical elements for high-performance computation and sensors. We prepared millimeter-scale objects (both polyhedra and more complex shapes designed to form an extended lattice), coated selected faces with a film

REPORTS

of low-melting, metallic alloy, and suspended the resulting particles in aqueous KBr solution at a temperature that melts the alloy. On agitation, the objects collide and interact through capillary forces between the drops of liquid alloy; self-assembly occurs because it minimizes the area of the interface between the alloy and the KBr solution and thus minimizes the free energy of the aggregate. The combination of the shapes of the objects, the pattern of the alloy-coated faces, and the shapes of the faces directs self-assembly and provides a strategy for controlling the structures of the resulting arrays.

This work builds on previous studies of 2D and 3D mesoscale self-assembly (1–8). In our studies of 2D systems, polymer plates floating at a perfluorodecalin/water interface interacted through lateral capillary forces; patterning the wettability of the surfaces of the plates directed the self-assembly (1). Achieving the same structural control in 3D self-assembly of small objects using capillarity is a more complicated problem—our previous work in 3D systems focused solely on simple tilings of space (4)—and requires a fluid-fluid interface with a high liquid-liquid interfacial free energy, a method to wet selected surfaces of the objects with only one of the liquids, and a procedure to freeze structures into mechanically stable forms once self-assembly is complete. We have addressed these issues by adapting a methodology originally used by Syms *et al.* to position the components of micromechanical assemblies (9). We used as liquid phases a low-melting alloy of bismuth, lead, tin, cadmium, and indium and aqueous KBr solution; the interface between these phases has a high interfacial free energy (we estimate this energy to be $\sim 400 \text{ mN m}^{-1}$) (10) primarily as a result of the high surface tension of molten alloy. We formed mesoscale objects of polyurethane (PU) by molding, and patterned their surfaces with alloy, by first attaching pieces of an adhesive-backed copper foil to the surfaces (Fig. 1) (11). The patterned copper surface coated spontaneously with thin films of alloy when dipped in molten alloy at 60°C . Self-assembly of the objects was accomplished by suspending and agitating them in an aqueous KBr solution at 60°C . After self-assembly was complete, the suspension was allowed to cool to room temperature. The alloy solidified and the resulting structures were mechanically stable (12).

Design of component pieces that self-assemble into open arrays of specified design requires two structural features to be correctly chosen: (i) the 3D shape of the pieces, and (ii) the positions and shapes of the alloy-coated faces on the surfaces of the objects. Here, we demonstrate that design based on these features allows the fabrication by self-assembly of a range of shapes, including

extended lattices, regular polyhedra, and open helices.

We chose regular polyhedra—octahedra, cubes, and tetrahedra—as the basis for the components for self-assembly of extended lattices and generated a new set of surface planes on them by truncating either their corners or edges. An important element of design in these systems was the shape of the alloy-coated surfaces of the mesoscopic objects (Fig. 2). Minimization of the area of the interface between the alloy and the aqueous KBr solution requires that the shapes of opposed faces between two objects match. Thus, the configurations suggested in Fig. 2, A and B, are energetically more favorable than those in Fig. 2, C and D, because they minimize the area of the alloy/aqueous KBr interface.

Both corner-truncated octahedra and edge-truncated cubes (Fig. 3) assembled into regular lattices: Truncated octahedra crystallized into a simple cubic lattice, and edge-truncated cubes formed a face-centered cubic lattice (Fig. 3, A to D); both used energetically favorable, area-minimizing configurations of the opposed faces (Fig. 2, A and B).

Both corner-truncated cubes and corner-truncated tetrahedra had triangular truncation planes covered with alloy (Fig. 3, E and G),

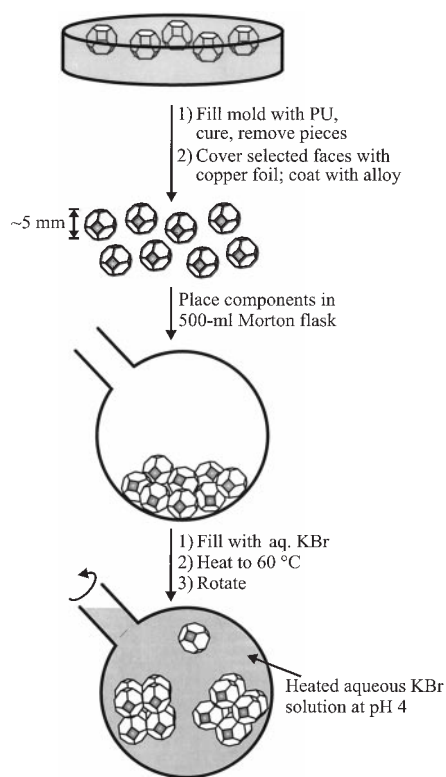


Fig. 1. Schematic diagram describing the process used to allow self-assembly of $\sim 5\text{-mm}$ polyhedra, having selected faces covered with low-melting metallic alloy. The liquid used to suspend these objects was saturated aqueous KBr solution.

and their shape, and the positions of the alloy-coated faces, prohibit the formation of an extended lattice with matching face profiles (such as in Fig. 2A). The corner-truncated tetrahedra assembled with matched configurations of the alloy-coated surfaces (Fig. 2A) and did not give an extended structure; rather, the pieces formed dodecahedra composed of five-membered rings of tetrahedra (Fig. 3F). In contrast, the corner-truncated cubes assembled into an extended lattice (Fig. 3H) but with unmatched configurations of the alloy-coated surfaces (Fig. 2C). These latter arrays are based on energetically less-favorable configurations of the opposed faces and, unlike the other arrays described in this study, had defects. These defects formed in the outer layer of components of the self-assembled structure when a component piece bonded to the structure with matched face profiles; only $\sim 2\%$ of the sites in the structure were defective.

Structures with matching face profiles were formed from the corner-truncated cubes when only four of the truncation planes, arranged tetrahedrally on the surface of each cube, were coated in alloy (Fig. 3, I and J). The cubes first formed five-membered rings with matching face profiles, and then dodecahedra analogous to those formed by the truncated tetrahedra. Five-membered rings formed only when four truncation planes were covered with alloy; when all eight corners were covered with alloy (Fig. 3, G and H), no dodecahedra formed. The additional alloy-covered truncation planes interfere with the formation of structures with matched face profiles, and complete opposition of the alloy-covered surfaces (to minimize the area of the interface of the alloy and aqueous solution) required formation of extended lattices, albeit at the cost of energetically unfavorable configurations of the opposed faces (Fig. 2C).

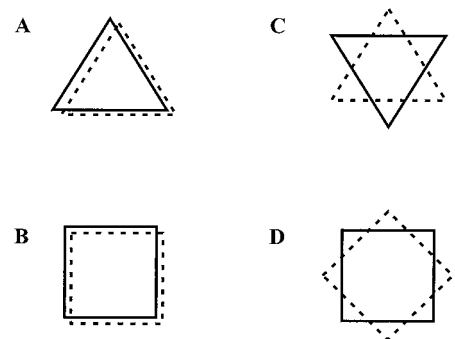


Fig. 2. Diagram depicting the opposition of triangular and square matched (A and B) and unmatched (C and D) faces; the solid and dotted lines represent the two opposed faces. The matched configurations (A and B) result in smaller areas for the interface between alloy and aqueous solution than do those that are unmatched (C and D); they are therefore energetically more favorable.

Fig. 3. Open lattice structures formed by self-assembly of polyhedra having selected faces coated with liquid alloy on agitating in aqueous KBr solution. (A) A drawing of a truncated octahedron (the region coated with alloy is shaded). (B) An array of 100 of the pieces depicted in (A) packed in a simple cubic lattice. (C) A drawing of an edge-truncated cube. (D) An array of 100 of the pieces depicted in (C) packed in a face-centered cubic lattice. (E) A drawing of a corner-truncated tetrahedron. (F) A dodecahedron assembled from 20 of the pieces depicted in (E). (G) A drawing of a corner-truncated cube. (H) An array of 100 of the pieces depicted in (G) packed in a body-centered cubic lattice. (I) A drawing of a corner-truncated cube with four alloy-coated truncation planes arranged tetrahedrally on the surface. (J) A dodecahedron assembled from 20 of the pieces depicted in (I).

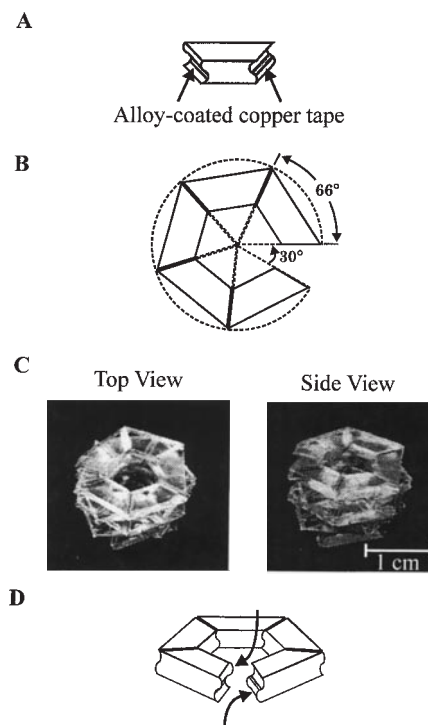
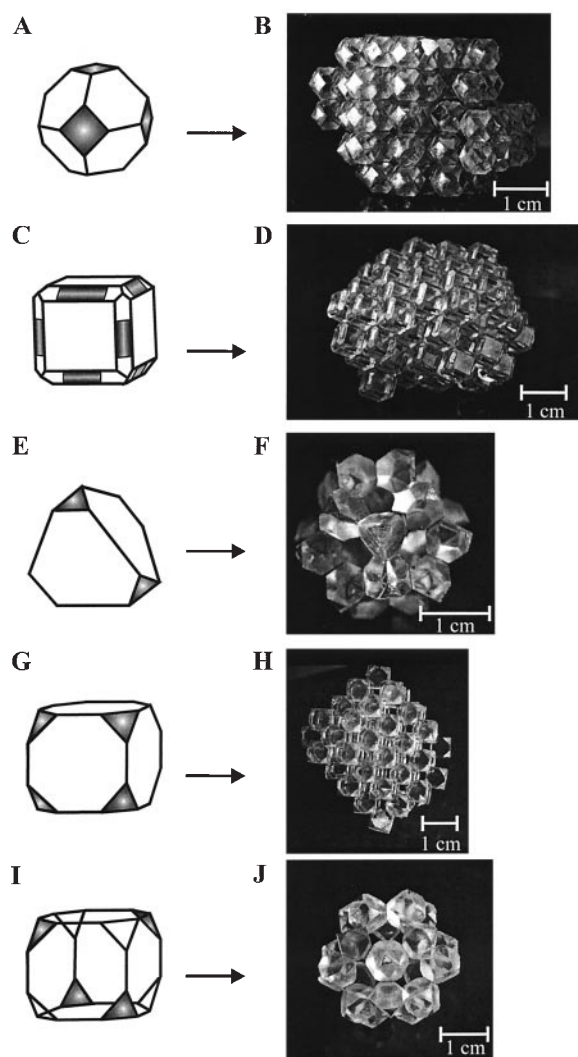


Fig. 4. A self-assembled helix. (A) A drawing of the shape designed to assemble into a helix. (B) A drawing of the top view of an assembly of five pieces showing the angles that the pieces describe. (C) A self-assembled helix (front and side views). (D) Diagram showing how the handedness of the self-assembled helix is established. The arrows indicate the two possible paths of approach taken by an incoming piece.

We extended the strategies illustrated by the regular crystalline lattices to a more complex structure, that is, a helix (Fig. 4). The components were designed to control both the direction of growth of the helix (so that it was along the length of the helix) and its handedness. The shapes used to form the helix incorporated three features. First, rectangles of alloy were placed on the sides of the components. Second, each piece subtended an angle of 66° when projected along the axis of the helix; thus, assembly of six pieces resulted in 1.1 turns of the helix. Third, the components had S-shaped sides and were chiral. The aggregates that formed had helical structures and the correct handedness, but were limited to ~ 18 objects (\sim three turns of the helix). We believe the size of these structures was limited by shear forces encountered during agitation and assembly.

A strategy based on minimizing the interfacial free energy of the interface between metallic alloy and aqueous KBr allows the self-assembly of open structures, with complexity extending from regular lattice structures to helices. Successful design requires control of the

shape of the objects, the placement of the surfaces supporting liquid alloy, and the shape of these surfaces. The number of alloy-coated faces per component is a factor that is independent of the shape of the faces; it controls the matching of the face profiles and thus the structure of the aggregate.

We have observed reproducible formation of defect-free lattices of at least 100 pieces (13); we have not explored or defined the upper limit of the number of components that assemble before defects begin to appear because of the time it takes to fabricate pieces. These structures are free of defects commonly found in 2D self-assembled structures (14) and in 3D self-assembled arrays of cubes (4). We attribute the reduction in defect density to two facts. First, it is easier to form defect-free 3D structures than 2D structures because there are more interconnections and components in 3D structures to cause alignment of the components. Second, the high interfacial free energy of the alloy-aqueous KBr system results in bonds between components that are strong enough to prevent slip dislocations.

This system—polyhedra designed to self-

assemble, molded in organic polymers, and connected through the use of capillary forces determined by minimization of the interfacial area between an alloy and aqueous KBr solution—is suitable for fundamental studies of self-assembly. The open lattice mesostructures with metallic interconnects that it generates also represent a step toward new types of structural materials, optical band-gap materials and other diffractive optical structures, and self-assembled, 3D microelectronic devices with built-in channels for cooling (15). The successful generation of these aggregates of millimeter-scale components suggests self-assembly as a strategy for precision assembly. To make the transition from fundamental studies to applications, we will require improved methods of fabrication of the components, methods of fabricating smaller components, and stronger adhesion between the components and the metallic alloy patterned on their surfaces.

References and Notes

1. N. Bowden, A. Terfort, J. Carbeck, G. M. Whitesides, *Science* **276**, 233 (1997).
2. A. Terfort, N. Bowden, G. M. Whitesides, *Nature* **386**, 162 (1997).
3. A. Terfort and G. M. Whitesides, *Adv. Mater.* **10**, 470 (1998).
4. J. Tien, T. L. Breen, G. M. Whitesides, *J. Am. Chem. Soc.* **120**, 12670 (1998).

Requirement for Type 2 NO Synthase for IL-12 Signaling in Innate Immunity

Andreas Diefenbach,^{1*} Heike Schindler,¹ Martin Röllinghoff,¹ Wayne M. Yokoyama,² Christian Bogdan^{1†}

Interleukin-12 (IL-12) and type 2 NO synthase (NOS2) are crucial for defense against bacterial and parasitic pathogens, but their relationship in innate immunity is unknown. In the absence of NOS2 activity, IL-12 was unable to prevent spreading of *Leishmania* parasites, did not stimulate natural killer (NK) cells for cytotoxicity or interferon- γ (IFN- γ) release, and failed to activate Tyk2 kinase and to tyrosine phosphorylate Stat4 (the central signal transducer of IL-12) in NK cells. Activation of Tyk2 in NK cells by IFN- α/β also required NOS2. Thus, NOS2-derived NO is a prerequisite for cytokine signaling and function in innate immunity.

The innate immune response to bacteria and protozoan parasites is characterized by the rapid recognition of microbial antigens, after which activated inflammatory cells release soluble mediators and antimicrobial effector molecules (1). The early production of IL-12 by granulocytes, macrophages, or dendritic cells stimulates the cytotoxic activity of NK cells and enhances their release of IFN- γ . Along with IL-12, IFN- γ then facilitates the later development of type 1 T helper cells (T_H1 cells) that ultimately activate macrophages for the destruction of intracellular pathogens through cognate interactions and further secretion of IFN- γ (2). A key antimicrobial agent implicated in this killing process is nitric oxide (NO) generated from the amino acid L-arginine by the inducible isoform of NO synthase (called iNOS or NOS2) (3). NOS2-derived NO can also regulate T cell proliferation, cytokine production, apoptosis, and signaling activity in vitro (4–6) and in vivo (7–9). In genetically resistant mice cutaneously infected with the protozoan parasite *Leishmania major*, the inhibition of early parasite spreading, the up-regulation of IFN- γ , and the induction of NK cell cytotoxicity at day 1 of infection were abolished after genetic deletion or functional inactivation of NOS2 (9), a response that is similar to that of mice after neutralization of IL-12 (10). This suggests that NOS2 deficiency might affect the availability of IL-12. Although the baseline expression of IL-12 subunit p40 mRNA in naïve NOS2^{-/-} mice was lower as

compared to that of NOS2^{+/+} mice, the production of active IL-12 p70 heterodimers by inflammatory macrophages was not reduced in the absence of NOS2 (9). Thus, both NO/NOS2 and IL-12 regulate the innate response to *L. major*, but whether and how they might interact in vivo remained unknown. We show here that NO/NOS2 is an integral part of the IL-12 signaling cascade in NK cells and therefore constitutes a prerequisite for the function of IL-12 in innate immunity.

We initially analyzed whether responsiveness to exogenous IL-12 in vivo required NOS2 activity. Wild-type NOS2^{+/+} mice (129/SvEv \times C57BL/6) were cutaneously infected with *L. major* promastigotes (11). At 24 hours, the parasites were found at the site of inoculation and in the draining popliteal lymph node (pLN). In NOS2-deficient mice (9, 12), in contrast, the parasites were disseminated to visceral organs, even after treatment with IL-12 (13) (Fig. 1A). In genetically susceptible BALB/c mice, which lack functional IL-12 early during infection (10, 14), treatment with IL-12 prevented parasite spreading at day 1 of infection (Fig. 1A). However, simultaneous application of L-N⁶-iminoethyl-lysine (L-NIL) (13), a potent competitive inhibitor of NOS2 (9), reversed the protective effect of IL-12 (Fig. 1A). Treatment of NOS2^{+/+} mice with IL-12 increased expression of IFN- γ mRNA and NK cell cytotoxic activity in the pLN after infection, whereas no such effect was observed in NOS2^{-/-} mice or in NOS2^{+/+} mice injected with L-NIL (Fig. 1, B and C). Similar amounts of IL-12 receptor β 1 and β 2 mRNA (15) were detected in the pLN of NOS2^{+/+} and NOS2^{-/-} mice at day 1 of infection (Fig. 1D), indicating that the impaired parasite control, IFN- γ expression, and NK cell activity in NOS2^{-/-} mice at day 1 of infection (9) resulted from an inability to respond to IL-12 but not from a lack of IL-12

5. A. W. Simpson and P. H. Hodkinson, *Nature* **237**, 320 (1972).
6. S. T. Schober, J. Friedrich, A. Altmann, *J. Appl. Phys.* **71**, 2206 (1992).
7. C. A. Murray and D. G. Grier, *Annu. Rev. Phys. Chem.* **47**, 421 (1996).
8. A. van Blaaderen, R. Ruel, P. Wiltzius, *Nature* **385**, 321 (1997).
9. P. W. Green, R. R. A. Syms, E. M. Yeatman, *J. Microelectromech. Syst.* **4**, 170 (1995).
10. We estimated the interfacial free energy of the alloy/ aqueous KBr interface using data from F. H. Howie and E. D. Hondros, *J. Mater. Science* **17**, 1434 (1982); M. A. Carroll and M. E. Warwick, *Mater. Sci. Technol.* **3**, 1040 (1987); and *Handbook of Chemistry and Physics*, D. R. Lide, Ed. (CRC Press, Boston, ed. 71, 1990), pp. 4-137 to 4-143. A liquid with a lower surface tension, such as the hydrophobic lubricant used in (2) and (4), was unable to generate capillary forces that were strong enough to hold objects together.
11. The designs selected for the components were used to fabricate machined aluminum masters; these masters were used to fabricate an elastomeric mold. We placed the masters in a petri dish, covered them with a liquid polydimethylsiloxane prepolymer (Sylgard 184, DuPont), and cured the prepolymer with heat (60°C, 30 min). Subsequent removal of the aluminum masters left an elastomeric mold consisting of wells in the shape of the aluminum masters. We filled the wells with a liquid PU prepolymer (NOA 73, Norland), cured the polymer by exposure to ultraviolet light (45 min), and removed the solid PU pieces. We patterned selected faces of these objects using adhesive copper foil (Scotch Brand Electrical Tape, 3M Corp., St. Paul, MN). This tape was cut to size and applied to the selected planes (or portions of these planes) of the polyhedra. This process was labor-intensive and limited the number of objects we were willing to examine in any experiment; it also limited these objects to sizes greater than 5 mm. The pattern of copper foil was coated with molten alloy (Bismuth Alloy 117, melting point: 47°C, Small Parts, Miami Lakes, FL) by dipping the pieces into a beaker containing molten alloy (under an aqueous acetic acid solution at pH 4 to dissolve oxidized alloy). Cooling left the faces of the copper foil coated with a film (~0.5 mm thick) of solid alloy. Self-assembly was allowed to take place in a 500-ml Morton flask filled with an aqueous solution of KBr. Acetic acid (3 ml) was added to dissolve oxide from the surface of the alloy. The flask and its contents were rotated horizontally with a rotary evaporator motor at 5 to 10 rpm and heated to 60°C in an oil bath. A typical assembly was complete after ~1 hour of agitation. We reduced the intensity of agitation about halfway through the experiment to obtain complete assemblies of the component pieces by increasing the concentration and thus the density (ranging from 1.1 to 1.3 g/ml) of the aqueous KBr solution.
12. Fragility resulted from delamination of tape from polymer, not fracture of alloy connections.
13. We assembled each array twice (with the exception of the dodecahedra, which were assembled three times). With the exception of the dodecahedra, the arrays incorporated all the starting pieces; for the dodecahedra, an excess of pieces was required. If we broke apart an array during assembly with a brief increase in rotation speed, the resulting fragments reassembled into a crystalline, monolithic array in ~1 hour.
14. N. Bowden, I. S. Choi, B. Grzybowski, G. M. Whitesides, *J. Am. Chem. Soc.*, in press.
15. G. M. Whitesides, *Sci. Am.* **273**, 146 (September 1995).
16. We thank S. Brittain for photography and K. Paul for discussions. Supported by the DARPA and the NSF. T.L.B. and S.R.J.O. thank the NSERC of Canada for postdoctoral fellowships; J.T. acknowledges the NSF for a predoctoral fellowship. T.H. was supported by the MRSEC program of the NSF under award number DMR-9400396.

9 February 1999; accepted 29 March 1999

¹Institut für Klinische Mikrobiologie, Immunologie und Hygiene, Universität Erlangen, Wasserturmstrasse 3, D-91054 Erlangen, Germany. ²Howard Hughes Medical Institute, Rheumatology Division Box 8045, Washington University School of Medicine, 660 South Euclid Avenue, St. Louis, MO 63110, USA.

*Present address: Department of Molecular and Cell Biology and Cancer Research Laboratory, 485 LSA, University of California, Berkeley, CA 94720, USA.

†To whom correspondence should be addressed. E-mail: christian.bogdan@mikrobio.med.uni-erlangen.de